nature COMMUNICATIONS

ARTICLE

Received 5 Sep 2015 | Accepted 11 Feb 2016 | Published 4 Apr 2016

DOI: 10.1038/ncomms11014 OPEN

Subterahertz dielectric relaxation in lead-free $Ba(Zr,Ti)O_3$ relaxor ferroelectrics

D. Wang[1], A.A. Bokov[2], Z.-G. Ye[1,2], J. Hlinka[3] & L. Bellaiche[4]

Relaxors are complex materials with unusual properties that have been puzzling the scientific community since their discovery. The main characteristic of relaxors, that is, their dielectric relaxation, remains unclear and is still under debate. The difficulty to conduct measurements at frequencies ranging from $\simeq$1 GHz to $\simeq$1 THz and the challenge of developing models to capture their complex dynamical responses are among the reasons for such a situation. Here, we report first-principles-based molecular dynamic simulations of lead-free $Ba(Zr_{0.5}Ti_{0.5})O_3$, which allows us to obtain its subterahertz dynamics. This approach reproduces the striking characteristics of relaxors including the dielectric relaxation, the constant-loss behaviour, the diffuse maximum in the temperature dependence of susceptibility, the substantial widening of dielectric spectrum on cooling and the resulting Vogel–Fulcher law. The simulations further relate such features to the decomposed dielectric responses, each associated with its own polarization mechanism, therefore, enhancing the current understanding of relaxor behaviour.

[1] Electronic Materials Research Laboratory—Key Laboratory of the Ministry of Education and International Center for Dielectric Research, School of Electronic and Information Engineering, Xi'an Jiaotong University, No. 28, Xianning West Road, Xi'an 710049, China. [2] Department of Chemistry and 4D LABS, Simon Fraser University, Burnaby, British Columbia, Canada V5A 1A6. [3] Department of Dielectrics, The Czech Academy of Sciences, Na Slovance 2, CZ-182 21 Praha 8, Czech Republic. [4] Department of Physics and Institute for Nanoscience and Engineering, University of Arkansas, Fayetteville, Arkansas 72701, USA. Correspondence and requests for materials should be addressed to D.W. (email: dawei.wang@mail.xjtu.edu.cn) or to A.A.B. (email: abokov@sfu.ca).

Relaxor ferroelectrics are fascinating materials whose major unusual characteristics are related to dipolar relaxation, hence the name relaxor given to them. Such relaxation manifests itself by the fact that the real part of their dielectric response versus temperature exhibits a broad peak, at $T = T_m$, which is strongly frequency dependent[1,2]. The origin of this dipolar relaxation is still open for discussion. A commonly proposed explanation is that it arises from the motion of polar nanoregions (PNRs), which appear on cooling at the so-called Burns temperature, T_B (refs 3–5). However, such a widely accepted mechanism has been recently challenged in (lead-based) relaxors on the ground of analysis of measured structural data[6–8] (note that the controversy also extends to atomistic simulations, since some computational works did report the existence of PNRs in relaxor ferroelectrics[4,9,10] while others did not[11–13]). This lack of consensus is largely due to the experimental challenges in observing PNRs directly and measuring some properties they are expected to exhibit, such as the dielectric spectra for frequencies ranging between 10^9 and 10^{12} Hz. As a matter of fact, while low frequencies (typically between 10^{-3} and 10^9 Hz) can be accessed by dielectric spectroscopy and high frequencies (typically phonons with frequencies above 10^{12} Hz) by the infrared reflectivity technique[2,14–17], very little data at limited temperatures are currently available, primarily from time-domain terahertz transmission spectroscopy[15,16], in the intermediate frequency range 10^9–10^{12} Hz. As a result, details of the relaxation spectrum (and, consequently, the details of the dipolar dynamics) remain unknown at $T \simeq T_B$, where relaxation exists at subterahertz frequencies only. At lower temperatures, the part of the spectrum where relaxation and phonon dynamics merge, is thus also poorly understood.

This article reports first-principles-based simulations on the lead-free $Ba(Zr_{0.5}Ti_{0.5})O_3$ (BZT) relaxor ferroelectrics in the subterahertz frequency range that resolve this outstanding problem. Atomistic features of our numerical tool further reveal the role of the Ti- and Zr-centred dipoles, and their cross-correlations in determining some relaxor characteristics such as the Vogel–Fulcher law (VF) obeyed by T_m. Note that BZT is chosen here because $BaTiO_3$-based relaxors proved both experimentally[5,17] and theoretically[4,18–20] to exhibit PNRs and because some experimental data on BZT (to test the predictions against) are available at some terahertz and subterahertz frequencies.

Results

Dielectric response. As indicated in the Methods section below, molecular dynamics simulations using the effective Hamiltonian of ref. 4 are conducted to predict the complex dielectric response at given temperatures. Practically, a series of molecular dynamics simulations is performed at 50 different temperatures between 5 and 1,000 K. After computing the dielectric response via equation (2) indicated in the Methods section, we analyse the obtained spectrum at each temperature. To this end, we apply an approach that is typically used in experimental dielectric spectroscopy, that is, to fit the data with an analytical expression written as a sum of standard empirical functions, each of which is the contribution of a particular polarization mechanism. We use the following expression (for the average diagonal element of the dielectric tensor):

$$\begin{aligned}\chi &= \chi_R + \chi_{COR} + \chi_{DHO_1} + \chi_{DHO_2} \\ &= \frac{\chi_{RO}}{\left[1+(iv/v_{HN})^{1-\alpha}\right]^{\gamma}} \\ &+ \frac{S_{CO}v_{CO}^2}{v_{CO}^2 - v^2 - iv\gamma_{CO} - v_{CR}\delta^2/(v_{CR}-iv)} \\ &+ \sum_{k=1,2}\frac{S_k v_k^2}{v_k^2 - v^2 - i\gamma_k v}.\end{aligned} \quad (1)$$

The first term of this sum is the Havriliak–Negami (HN) function, which represents a relaxation mechanism. In this function, α and γ are parameters characterizing the shape of the relaxation spectrum, and χ_{RO} and v_{HN} are the dielectric strength and the characteristic frequency of this relaxation mechanism, respectively. The second term of equation (1) describes a coupled oscillator-relaxator (COR) mechanism, with S_{CO}, v_{CO}, and γ_{CO} being the dielectric strength, resonant frequency and damping constant of the coupled oscillator mode, respectively, while v_{RO} is the bare relaxation frequency of the coupled relaxation mode and δ is the coupling constant characterizing the strength of interaction between the oscillator and the relaxator. The last two terms represent two damped harmonic oscillators (DHO) of dielectric strength S_k, resonant frequency v_k and damping constant γ_k, with $k = 1, 2$. Note that, during our nonlinear least square fitting procedure, the real and imaginary parts are fitted simultaneously in the entire frequency range varying between 10^9 and 2×10^{13} Hz (0.033–667 cm^{-1}), where meaningful data are available.

The simulated spectra and the results of their fitting to equation (1) are shown for selected temperatures in Fig. 1 (fitting results at some other temperatures can be found in the Supplementary Movie 1). One can see that, in all cases, the isothermal frequency dependence of the complex total susceptibility can be well described by equation (1), which justifies the choice of such an equation. Figure 1 further provides the decomposition of χ into four separate terms of equation (1), and thereby demonstrates that χ_R is the dominant effect for the lowest frequencies, while χ_{COR} and the DHOs contribute to the dielectric response for the intermediate and highest frequencies, respectively. Note that, at microscopic level, our simulations reveal that the intermediate DHO_1 mode is mostly related to the phonon vibration of the Zr ions, while the DHO_2 mode is associated with the high-frequency phonon vibrations of the Ti ions, which is consistent with ref. 20. The COR mechanism corresponds to a mixed relaxation-oscillation mode within the Ti subsystem, that is a single Debye relaxation mode coupled to an optical phonon mode, while the HN function corresponds to a more complex relaxation mode arising from the influence of different chemical environments on Ti-centred dipoles. Moreover, Fig. 1c,d also display the experimental data at 150 K of ref. 16 by means of triangles. The agreement between the simulations and the measured data is quite remarkable for both the real and imaginary parts of the dielectric response, especially given that Fig. 1 shows that these two parts are very sensitive to temperature. Such an agreement asserts the validity and accuracy of the present simulations.

Relaxation. Having demonstrated the accuracy of our simulation, let us now use the best-fit relaxation parameters of equation (1) to calculate $\chi(T, v)$ at selected temperatures and probing frequencies. The resulting real and imaginary parts of this total dielectric response as a function of temperature are reported in Fig. 2a,b, respectively, for different frequencies ranging from 1 GHz to 1 THz. One can see that both the real and imaginary parts of the predicted dielectric response exhibit a broad peak over temperature, which shifts in position when the probing frequency changes. In other words, our present first-principles-derived simulations reproduce the main characteristics (dielectric dispersion) of relaxor ferroelectrics. Moreover, Fig. 2b also reveals that the simulated imaginary part of the dielectric response is practically insensitive to frequency for low temperatures (below ~150 K), which is experimentally known to occur in relaxor ferroelectrics[21,22], and is often referred to as the constant-loss behaviour.

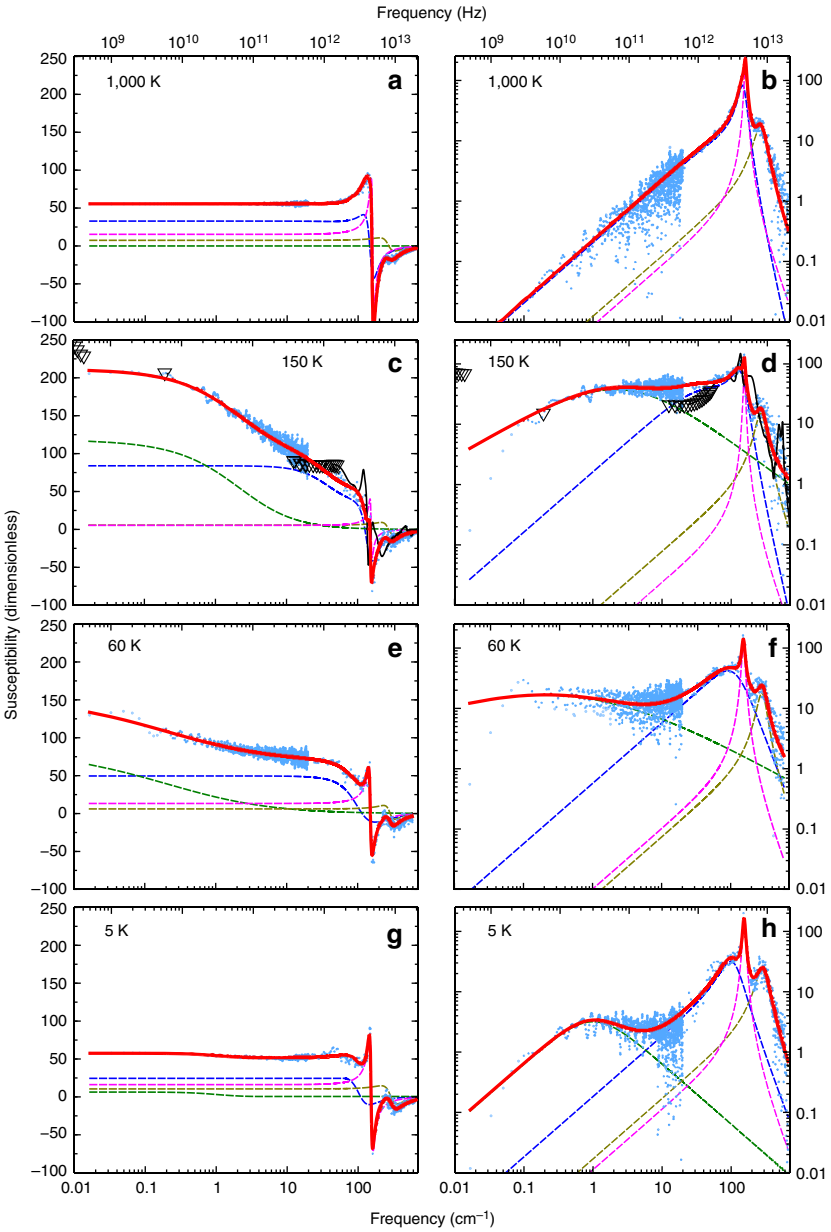

Figure 1 | Dielectric relaxation spectra of the compositionally disordered $Ba(Zr_{0.5}Ti_{0.5})O_3$ crystal at selected temperatures. (**a**–**h**) Frequency dependence of real (**a**,**c**,**e**,**g**) and imaginary (**b**,**d**,**f**,**h**) parts of the dielectric susceptibility at 1,000 K (**a**,**b**), 150 K (**c**,**d**), 60 K (**e**,**f**) and 5 K (**g**,**h**). The blue symbols are the results of molecular dynamics simulations; for the sake of clarity, every point at $\nu \gtrsim 20\,cm^{-1}$ represents the average value over 100 neighbouring simulation points. The thick red line is the fit to equation (1); green, blue, magenta and olive dashed lines show the contributions of relaxation and oscillation mechanisms, χ_R, χ_{COR}, χ_{DHO_1} and χ_{DHO_2}, respectively, that comprise the total response. The triangles and thin black lines in **c**,**d** are the experimental data for the ceramic $Ba(Zr_{0.6}Ti_{0.4})O_3$ of close composition taken from fig. 5 of ref. 16. Note that between 0.01 and 7 cm^{-1} only one experimental point (at 0.2 cm^{-1}) is available, which makes it impossible to determine reliably the parameters of the relaxation process based on experimental data.

Figure 2a also displays the dielectric response obtained from the extrapolation of our numerical molecular dynamics data down to zero frequency, that is the dielectric response given by $\chi_{RO} + \chi_{COR}(\nu = 0) + S_1 + S_2$, along with the dielectric response obtained from our previous effective Hamiltonian simulations using the Monte–Carlo method[4]. Interestingly, as evidenced in Fig. 2a, such two static responses agree very well with each other, which further supports the scheme described by equation (1) to fit the molecular dynamics outputs. In particular, these two responses are found to possess a maximum at some finite temperature (of the order of 100 K), similar to the peak experimentally found for the static susceptibility in some lead-based and lead-free relaxors[2,22,23].

Fitting parameters. To gain a deeper insight into the results depicted in Fig. 2a,b, we take a close look at the temperature dependences of some parameters appearing in equation (1). Such dependences are shown in Fig. 3. More precisely, Fig. 3a reports the total static susceptibility, $\chi(\nu = 0)$, associated with equation (1), as well as its separate contributions from the mechanisms involving relaxation, that is, $\chi_{RO} + \chi_{COR}(\nu = 0)$.

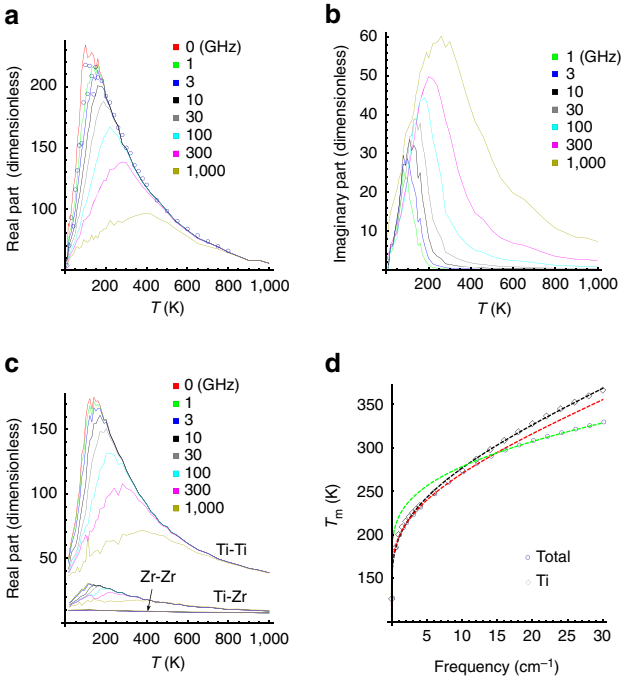

Figure 2 | Temperature dependences of the complex susceptibility for different probing frequencies and the fitting to the VF law. (**a**) Real part of the total susceptibility. Results obtained from previous Monte-Carlo method simulations[4] are also shown as blue circles. (**b**) Imaginary part of the total susceptibility. (**c**) Different contributions to the real part of total susceptibility (from top to bottom): $\chi^{Ti,Ti}$, $\chi^{Ti,Zr}$, $\chi^{Zr,Zr}$. (**d**) Frequency dependence of the temperatures at which the real parts of χ and $\chi^{Ti,Ti}$ are maximum (hollow circles and diamonds, respectively), with the solid lines fitting these curves to the VF laws.

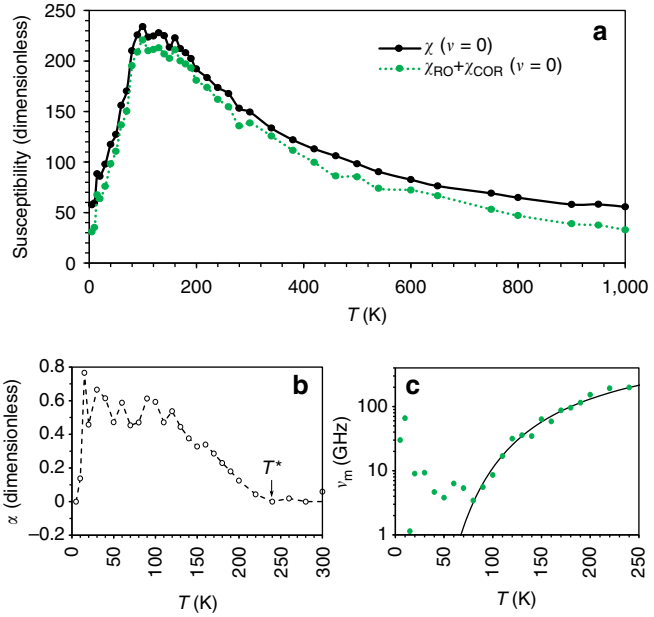

Figure 3 | Parameters of the dielectric spectra in the compositionally disordered $Ba(Zr_{0.5}Ti_{0.5})O_3$ crystal as functions of temperature. (**a**) Total static susceptibility χ ($\nu = 0$), and static susceptibility related to all polarization processes in which relaxation is involved, $\chi_{RO} + \chi_{COR}$ ($\nu = 0$). (**b**,**c**) Parameters of the HN relaxation process: the parameter α, characterizing the width of relaxation spectrum (**b**) and the most probable relaxation frequency, ν_m (**c**). The dashed line in **b** is the guide to the eyes and the solid line in **c** is the fit to the Arrhenius law.

Figure 3b displays the α parameter associated with the HN function (equation (1)), while Fig. 3c shows the frequency, ν_m, at which $\mathrm{Im}\chi_R(\nu)$ peaks for any given temperature (ν_m is known as the most probable relaxation frequency and may differ from ν_{HN}). The Supplementary Fig. 1 and Supplementary Note 1 provide information about other parameters not shown in Fig. 3. It is clear from Fig. 3a that, for temperatures above the well-known Burns temperature $T_B \simeq 450$ K of this system[4,17], the total static dielectric susceptibility is dominated by the relaxation mechanisms, or, equivalently, that the DHOs contribute only very slightly to it (the contribution from DHOs is the difference between the black and green curves of Fig. 3a, which is found to be ~ 20 for any investigated temperature). Such features contrast with the case of lead-based perovskite relaxors, where the response is purely of phonon (DHO) nature for $T > T_B$ and relaxation appears only at $T < T_B$ (refs 24,25). The large and small contributions of the relaxation mechanisms and the DHOs, respectively, result in the Curie–Weiss law behaviour for $T > T_B$ with a negative critical temperature, T_{CW}, in agreement with the Monte–Carlo method simulations[4] and experimental results[17]. Moreover, $\chi_{RO} + \chi_{COR}(\nu = 0)$ exhibits a peak at $T \simeq 100$ K, which is found to be fully responsible for the maximum in the temperature dependence of the total static susceptibility reported in Fig. 2a (note also that the broadness aspect of the total susceptibility is found to originate from the temperature behaviour of the static contributions of the relaxation mechanisms). Supplementary Fig. 1 further shows the separate contribution of $\chi_{COR}(\nu = 0)$ and χ_{RO} as a function of temperature. In particular, χ_{RO} is found to practically vanish for temperatures above T_B (implying that the COR mechanism is the most predominant player there), while χ_{RO} is about twice as big as $\chi_{COR}(\nu = 0)$ for temperatures close to 100 K. However, we numerically found that the HN and COR contributions significantly overlap in frequency, especially at comparatively high temperatures. As a result, some of the parameters of these two contributions can only be estimated rather than reliably determined. One should therefore consider the temperature dependence of the sum of χ_{RO} and χ_{COR} rather than look at them separately. This explains why this sum is shown in Fig. 3a.

It is also important to realize that Fig. 3b reveals that the α parameter departs from zero at the temperature of $\simeq 240$ K, that is, at the so-called T^* characteristic temperature of BZT, below which Ti-rich PNRs were found to begin interacting with each other in an antiferroelectric-like fashion in ref. 4. This departure from zero may indicate the existence of a distribution of Debye modes with different relaxation times. α then increases up to $\simeq 0.5$ when cooling the system from T^* to $\simeq 130$ K. It remains quite large when further decreasing the temperature down to 5–10 K, which results in frequency broadening of the $\mathrm{Im}\chi_R(\nu)$ peak. In fact, the peak becomes so wide at temperatures below $\simeq 100$ K (Fig. 1f) that the loss is practically constant with frequency (cf. Fig. 2b). Note that the broadening of relaxation spectrum on cooling and the constant-loss behaviour are two characteristic features of relaxor ferroelectrics, in contrast to the behaviour of most other dielectrics where the shape of the spectrum is temperature independent[26]. Figure 3b,c also indicate that the extracted α and ν_m parameters exhibit some scattering for temperatures ranging between $\simeq 15$ and 80 K. This is because the characteristic relaxation frequency, ν_m, reaches the low-frequency boundary of the available molecular dynamics data in that temperature range (as shown in Fig. 3c) and, as a result, the HN parameters become uncertain. On the other hand, at the very low temperatures of 5–10 K, the relaxation response moves back to the simulation frequency window, as evidenced in Fig. 1g,h, which allows us to precisely extract again the values of α.

Interestingly, this parameter is now very close to zero as revealed by Fig. 3b, which explains why the loss peak is now narrower (cf. Fig. 1h) and which is characteristic of a simple Debye (exponential in time domain) relaxation. Note that the remaining relaxation at this temperature is numerically found to be caused by dipoles associated with Ti ions surrounded mostly by Zr ions (not shown here).

Arrhenius and VF laws. Let us now discuss the temperature dependence of ν_m depicted in Fig. 3c. Fitting this relation for temperatures above 70 K with the VF law, $\nu_m = \nu_a \exp[-E_a/k_B(T-T_0)]$ shows that $T_0 = (-2 \pm 9)$ K, that is, T_0 can be safely assumed to vanish. In other words, ν_m rather follows an Arrhenius law $\nu_m = \nu_a \exp(-E_a/k_BT)$ above $\simeq$70 K, with the best-fit parameters $\nu_a = 1.6 \times 10^{12}$ Hz (53 cm^{-1}) and $E_a = 0.043$ eV. Interestingly, an Arrhenius law having a similar ν_a, but four times larger E_a, has been experimentally found in BZT (refs 15,16) for a different, lower-in-frequency relaxation mode. The fact that both the present simulations and the experiments indicate that T_0 vanishes (that is, it is not finite) in BZT can be understood in terms of the semi-phenomenological model proposed by Pirc and Blinc[27]. This model suggests that T_0 corresponds to the temperature at which the PNRs grow into an infinite cluster as temperature decreases, which explains why some relaxor systems exhibit a VF law behaviour. Such a scenario is relevant to lead-based relaxors according to a recent study[28]. However, PNRs in BZT are confined to Ti-rich regions and cannot grow into an infinite cluster with decreasing temperature (cf. ref. 4) because these PNRs are immersed into a Zr-rich matrix that is only weakly polarizable. Consistent with the fact that Pirc and Blinc have shown that the VF law would reduce to the Arrhenius law if PNRs did not grow, we can conclude that the Arrhenius law, rather than the VF law, applies to BZT. Note that Fig. 3c further shows that the Arrhenius law is not obeyed at lower temperatures, which is consistent with ref. 20.

Furthermore, the data displayed in Fig. 2a also allow us to obtain the temperature, T_m, at which the real part of the dielectric response peaks, for any probing frequency, ν (the T_m versus ν for the imaginary part of the susceptibility is shown in Supplementary Fig. 2 and discussed in Supplementary Note 2). The dependence of T_m on ν is reported in Fig. 2d, and it neither follows Arrhenius behaviour nor a single VF relation. In fact, Fig. 2d shows that T_m obeys two different VF laws of the form $\nu = \nu_0 \exp[-U/(T_m - T_{VF})]$: one for temperatures below $\simeq$280 K (with the best-fit parameters $\nu_0 = 322$ cm^{-1}, $U = 637$ K and $T_{VF} = 87$ K) and one for temperatures above it ($\nu_0 = 1{,}950$ cm^{-1}, $U = 1{,}005$ K and $T_{VF} = 88$ K). These two VF laws have significantly different U and ν_0, but similar $T_{VF} \simeq 90$ K. Interestingly, this temperature is consistent with the finding in ref. 4 that the thermally activated reorientations of the (Ti-based) dipoles inside the existing PNRs are numerically found to be frozen in BZT below $\simeq$90 K. This T_{VF} is also close to the temperature of the static susceptibility maximum shown in Figs 2a and 3a, as predicted by the phenomenological theory of VF relationship for relaxors proposed by Tagantsev[29]. In particular, it is interesting to realize that refs 22,29 indicate that T_m can follow a VF law even if the characteristic relaxation frequency obeys the Arrhenius behaviour provided that the static dielectric response possesses a maximum at a finite temperature, which is consistent with the present data shown in Fig. 2d (for T_m), Fig. 3c (for ν_m) and Fig. 2a (for the static dielectric response). Note that Tagantsev's model predicts the fulfillment of a single VF law for the $T_m(\nu)$ values belonging to the temperature interval above $T_m(\nu = 0)$, but neither the size of this interval nor the $T_m(\nu)$ behaviour at higher temperatures are specified (they are determined by several factors including the shape of temperature dependence of static susceptibility, the temperature dependence of characteristic times of the contributing relaxation modes, and the shape of relaxation spectrum[22]). In fact, two different VF laws have been observed experimentally in some relaxors[30], with the second VF law occurring in a higher temperature range that cannot be described by Tagantsev's model.

It is also worth emphasizing that, in Tagantsev's model for T_m, U is not an activation energy and T_{VF} is not the temperature where the relaxation frequency vanishes, that is, T_{VF} could be different from T_0 (the critical temperature involved in the temperature behaviour of ν_m), while in canonical lead-based relaxors these two temperatures are experimentally found to be close to each other. Therefore, like in other relaxors, the dielectric response in BZT differs fundamentally from that in ideal paraelectrics, where the static susceptibility and the characteristic relaxation time diverge simultaneously (in proportion to $1/T$) as the temperature approaches zero (ref. 26). However, in canonical lead-containing relaxors the relaxation time diverges at the characteristic VF temperature $T_0 > 0$ (ref. 21), while, in BZT, the relaxation time remains finite at $T > 0$, but the dielectric strength (static susceptibility) of relaxation mode peaks at another characteristic temperature, $T_m(\nu = 0) \simeq T_{VF}$, and tends towards zero on further cooling.

Note also that a detailed analysis (Supplementary Fig. 3 and Supplementary Note 3) shows that the two relaxation-related modes (HN and COR), we have predicted in our simulations, are also seen in experiments (they are traditionally called central modes). However, their behaviour cannot be accurately verified because of insufficiency of experimental data. Moreover, experiments also report an additional relaxation mode in BZT which dominates at very low frequency ($\nu < 1$ GHz). This latter mode cannot be mimicked by our present simulations and was suggested to originate from the collective dynamics inside PNRs or the thermally activated reorientations of the PNRs (ref. 20).

Atomistic decomposition. To elucidate further the origin of the dielectric response in BZT and to better understand the existence of two VF laws depicted in Fig. 2d, we take advantage of another strength provided by our atomistic simulations, that is the possibility to separate the total dielectric response into its constituent parts: the $\chi^{Ti,Ti}$ contribution from the 5-atom cells centred on Ti sites, the $\chi^{Zr,Zr}$ contribution from the 5-atom cells centred on Zr sites and the $\chi^{Ti,Zr}$ correlation between these two different types of 5-atom cells. This decomposition of the total dielectric response is (unfortunately) impossible to obtain in experiments but is made feasible here, thanks to the previously developed technique utilizing, in equation (2), the fact that $\mathbf{d} = \mathbf{d}^{Ti} + \mathbf{d}^{Zr}$, where $\mathbf{d}$ is the total electric dipole moment of the whole system, while $\mathbf{d}^{Ti}$ and $\mathbf{d}^{Zr}$ are the electric dipole moments of the 5-atom cells centred on the Ti and Zr ions, respectively[20] [note that the effective Hamiltonian used here[4] possesses the so-called local modes as degrees of freedom. These local modes are technically centred on the B-sites (Ti or Zr), represent the collective displacements of the Ba, B and oxygen ions within any 5-atom unit cell, and are directly proportional to the electric dipole moments of each 5-atom cell]. Figure 2c shows the resulting real parts of $\chi^{Ti,Ti}$, $\chi^{Ti,Zr}$ and $\chi^{Zr,Zr}$ as a function of temperature, for different probing frequencies. The real part of $\chi^{Ti,Ti}$ resembles the total susceptibility of Fig. 2a in every aspect except that its maximum value is $\sim$20% smaller. In contrast, the real parts of $\chi^{Ti,Zr}$ and $\chi^{Zr,Zr}$ are much smaller in both magnitude (approximately one tenth of $\chi^{Ti,Ti}$) and dispersion. In particular, the susceptibility of $\chi^{Zr,Zr}$ is essentially a constant over temperatures and frequencies. These results therefore

indicate that the total dielectric response of disordered BZT and its accompanying dispersion are mainly dominated by the response arising from the Ti-centred 5-atom cells, which is consistent with our aforementioned finding that the HN and COR mechanisms (which concern the Ti subsystem) are mostly responsible for the unusual dielectric features of BZT below T_B. Interestingly, one can also extract from Fig. 2c the temperature $T_{m,Ti}$ at which the real part of $\chi^{Ti,Ti}$ peaks for any probing frequency. The resulting $T_{m,Ti}$-versus-ν curve is also reported in Fig. 2d, and can be well fitted at any temperature by a single VF law, with the best-fit parameters $\nu_0 = 361\,cm^{-1}$, $U = 745\,K$ and $T_{VF} = 69\,K$. It is striking to realize that the $T_{m,Ti}(\nu)$ function is virtually identical to that of the total response for any temperature $\lesssim 240\,K$ (which is, incidentally, T^*), but differs for the temperatures above. For these higher temperatures, one can see in Fig. 2c that the real part of $\chi^{Ti,Zr}$ disperses much less than that of $\chi^{Ti,Ti}$, which leads to a reduction of T_m with respect to $T_{m,Ti}$ above 280 K.

Discussion

In summary, we report first-principles-derived simulations in BZT that reproduce the main characteristics of relaxor ferroelectrics, that is the frequency dependence of the real and imaginary parts of the dielectric response versus temperature. Analysis of these simulated results reveals that the relaxation-type polarization processes dominate in the dielectric response of disordered BZT for all temperatures, which contrasts with lead-based perovskite relaxors in which the response is purely of phonon nature for $T > T_B$ and the relaxation only appears below T_B (refs 24,25). Such a dramatic difference may originate from the fact that BZT has been reported to exhibit PNRs below T_B (refs 4,5,18–20), while the PNRs as compact regions of ferroelectric order might not exist inside a nonpolar matrix in the classical lead magnesium niobate relaxor according to recent diffuse neutron and x-ray scattering[6,7] and x-ray fluorescence holography experiments[8]. Furthermore, the significance of the characteristic relaxor temperature T^* of BZT in terms of dipolar relaxation is also clearly determined by the present study: above this temperature, the relaxation consists of a single Debye mode (corresponding to $\alpha = 0$) coupled to an optical phonon mode within the Ti subsystem, while below T^*, the Ti-centred dipoles subject to different chemical environments result in a relaxation spectrum that significantly broadens ($\alpha > 0$), signifying the distribution of Debye relaxation times. The present computational results also predict that the frequency dependence of the T_m temperature at which the real part of the total dielectric response peaks is well described (below $\simeq 280\,K$) by a single VF law. The second VF law having a different parameter U but identical T_{VF} is further found to describe the behaviour of T_m versus frequency for the temperatures above $\simeq 280\,K$. We therefore believe that the present study deepens our knowledge on relaxor ferroelectrics, in general, and their characteristic dipolar relaxations, in particular, which are responsible for their unusual properties.

Methods

First-principles model. We employ the first-principles-based effective Hamiltonian that has been developed in ref. 4 and successfully used to model and study different static and dynamical properties of the BZT systems[18–20]. This Hamiltonian is presently implemented within the molecular dynamics technique described in refs 20,31–35, and is applied to a $12 \times 12 \times 12$ supercell made from disordered $Ba(Zr_{0.5}Ti_{0.5})O_3$ solid solution. The complex dielectric susceptibility, $\chi_{lm}(\nu)$, can be obtained from the molecular dynamics simulations via refs 20,31,33,36,37:

$$\chi_{lm}(\nu) = \frac{1}{\varepsilon_0 V k_B T}\left[\langle d_l(t) d_m(t)\rangle + i2\pi\nu \int_0^\infty dt e^{i2\pi\nu t}\langle d_l(t) d_m(0)\rangle\right] \quad (2)$$

where ν is the frequency, while l and m define Cartesian components, V is the volume of the chosen supercell, ε_0 is the vacuum permittivity and $\mathbf{d}(t)$ is the electric dipole moment of the system at time t, and $\langle ... \rangle$ represents thermal averages. At any given time t, $\mathbf{d}(t)$ is obtained by summing over every dipole of the system, and therefore contains contributions from different compositional regions that have different dipole dynamics, including relaxational dynamics. Note the important technical differences with respect to previous studies[20,32–35,38,39]: the total molecular dynamics simulation time is extended to 16 ns, which is about eight times longer than the simulation time used in refs 20,32–35,38,39, to accurately mimic the low-frequency part of the dielectric response; and the real part of the dielectric response is presently investigated in detail, in addition to the imaginary part.

References

1. Colla, E., Koroleva, E., Okuneva, N. & Vakhrushev, S. Low-frequency dielectric response of $PbMg_{1/3}Nb_{2/3}O_3$. *J. Phys. Condens. Matter* **4,** 3671–3677 (1992).
2. Bokov, A. A., Maglione, M. & Ye, Z.-G. Quasi-ferroelectric state in $Ba(Ti_{1-x}Zr_x)O_3$ relaxor: dielectric spectroscopy evidence. *J. Phys. Condens. Matter* **19,** 092001 (2007).
3. Hiraka, H., Lee, S., Gehring, P., Xu, G. & Shirane, G. Cold neutron study on the diffuse scattering and phonon excitations in the relaxor $Pb(Mg_{1/3}Nb_{2/3})O_3$. *Phys. Rev. B* **70,** 184105 (2004).
4. Akbarzadeh, A., Prosandeev, S., Walter, E., Al-Barakaty, A. & Bellaiche, L. Finite-temperature properties of $Ba(Zr,Ti)O_3$ relaxors from first principles. *Phys. Rev. Lett.* **108,** 257601 (2012).
5. Xie, L. *et al.* Static and dynamic polar nanoregions in relaxor ferroelectric $Ba(Ti_{1-x},Sn_x)O_3$ system at high temperature. *Phys. Rev. B* **85,** 014118 (2012).
6. Bosak, A., Chernyshov, D. & Krisch, M. Diffuse scattering in relaxor ferroelectrics: true three-dimensional mapping, experimental artefacts and modelling. *Acta Crystallogr. A* **68,** 117–123 (2012).
7. Hlinka, J. Do we need the ether of polar nanoregions? *J. Adv. Dielectr.* **2,** 1241006 (2012).
8. Hu, W. *et al.* Acute and obtuse rhombohedrons in the local structures of relaxor ferroelectric $Pb(Mg_{1/3}Nb_{2/3})O_3$. *Phys. Rev. B* **89,** 140103 (R) (2014).
9. Tinte, S., Burton, B. P., Cockayne, E. & Waghmare, U. V. Origin of the relaxor state in $Pb(B_xB'_{1-x})O_3$ perovskites. *Phys. Rev. Lett.* **97,** 137601 (2006).
10. Paściak, M., Welberry, T. R., Kulda, J., Kempa, M. & Hlinka, J. Polar nanoregions and diffuse scattering in the relaxor ferroelectric $Pb(Mg_{1/3}Nb_{2/3})O_3$. *Phys. Rev. B* **85,** 224109 (2012).
11. Takenaka, H., Grinberg, I. & Rappe, A. M. Anisotropic local correlations and dynamics in a relaxor ferroelectric. *Phys. Rev. Lett.* **110,** 147602 (2013).
12. Grinberg, I., Shin, Y.-H. & Rappe, A. M. Molecular dynamics study of dielectric response in a relaxor ferroelectric. *Phys. Rev. Lett.* **103,** 197601 (2009).
13. Sepliarsky, M. & Cohen, R. E. First-principles based atomistic modeling of phase stability in PMN-*x*PT. *J. Phys. Condens. Matter* **23,** 435902 (2011).
14. Ke, S., Fan, H., Huang, H., Chan, H. & Yu, S. Dielectric dispersion behavior of $Ba(Zr_xTi_{1-x})O_3$ solid solutions with a quasiferroelectric state. *J. Appl. Phys.* **104,** 034108 (2008).
15. Nuzhnyy, D. *et al.* Broadband dielectric response of $Ba(Zr,Ti)O_3$ ceramics: from incipient via relaxor and diffuse up to classical ferroelectric behavior. *Phys. Rev. B* **86,** 014106 (2012).
16. Petzelt, J. *et al.* Broadband dielectric spectroscopy of $Ba(Zr,Ti)O_3$: dynamics of relaxors and diffuse ferroelectrics. *Ferroelectrics* **469,** 14–25 (2014).
17. Maiti, T., Guo, R. & Bhalla, A. Structure-property phase diagram of $Ba(Zr,Ti)O_3$ system. *J. Am. Ceram. Soc.* **91,** 1769–1780 (2008).
18. Prosandeev, S., Wang, D., Akbarzadeh, A., Dkhil, B. & Bellaiche, L. Field-induced percolation of polar nanoregions in relaxor ferroelectrics. *Phys. Rev. Lett.* **110,** 207601 (2013).
19. Prosandeev, S., Wang, D. & Bellaiche, L. Properties of epitaxial films made of relaxor ferroelectrics. *Phys. Rev. Lett.* **111,** 247602 (2013).
20. Wang, D. *et al.* Fano resonance and dipolar relaxation in lead-free relaxors. *Nat. Commun.* **5,** 5100 (2014).
21. Bokov, A. A. & Ye, Z.-G. Recent progress in relaxor ferroelectrics with perovskite structure. *J. Mater. Sci.* **41,** 31–52 (2006).
22. Bokov, A. A. & Ye, Z.-G. Dielectric relaxation in relaxor ferroelectrics. *J. Adv. Dielectr.* **2,** 1241010 (2012).
23. Bokov, A. A. & Ye, Z.-G. Double freezing of dielectric response in relaxor $Pb(Mg_{1/3}Nb_{2/3})O_3$ crystals. *Phys. Rev. B* **74,** 132102 (2006).
24. Bovtun, V. *et al.* Broad-band dielectric response of $PbMg_{1/3}Nb_{2/3}O_3$ relaxor ferroelectrics: Single crystals, ceramics and thin films. *J. Eur. Ceram. Soc.* **26,** 2867–2875 (2006).
25. Gehring, P. Neutron diffuse scattering in lead-based relaxor ferroelectrics and its relationship to the ultra-high piezoelectricity. *J. Adv. Dielectr.* **2,** 1241005 (2012).
26. Jonscher, A. *Dielectric Relaxation in Solids* (Chelsea Dielectrics Press, 1983).
27. Pirc, R. & Blinc, R. Vogel-Fulcher freezing in relaxor ferroelectrics. *Phys. Rev. B* **76,** 020101 (R) (2007).
28. Al-Barakaty, A., Prosandeev, S., Wang, D., Dkhil, B. & Bellaiche, L. Finite-temperature properties of the relaxor $PbMg_{1/3}Nb_{2/3}O_3$ from atomistic simulations. *Phys. Rev. B* **91,** 214117 (2015).

29. Tagantsev, A. Vogel-Fulcher relationship for the dielectric permittivity of relaxor ferroelectrics. *Phys. Rev. Lett.* **72,** 1100–1103 (1994).
30. Bokov, A. A., Leshchenko, M., Malitskaya, M. & Raevski, I. Dielectric spectra and Vogel-Fulcher scaling in $Pb(In_{0.5},Nb_{0.5})O_3$ relaxor ferroelectric. *J. Phys. Conden. Matter* **11,** 4899–4911 (1999).
31. Ponomareva, I., Bellaiche, L., Ostapchuk, T., Hlinka, J. & Petzelt, J. Terahertz dielectric response of cubic $BaTiO_3$. *Phys. Rev. B* **77,** 012102 (2008).
32. Wang, D., Weerasinghe, J., Bellaiche, L. & Hlinka, J. Dynamical coupling in $Pb(Zr,Ti)O_3$ solid solutions from first principles. *Phys. Rev. B* **83,** 020301 (R) (2011).
33. Wang, D., Weerasinghe, J., Al-barakati, A. & Bellaiche, L. Terahertz dielectric response and coupled dynamics of ferroelectrics and multiferroics from effective Hamiltonian simulations. *Int. J. Mod. Phys. B* **27,** 1330016 (2013).
34. Weerasinghe, J., Wang, D. & Bellaiche, L. Low-frequency coupled modes in disordered $Pb(Zr,Ti)O_3$ solid solutions from first principles. *Phys. Rev. B* **85,** 014301 (2012).
35. Weerasinghe, J., Wang, D. & Bellaiche, L. Effect of central mode on the dielectric tunability of ferroelectrics near room temperature: a first-principle-based study. *J. Phys. Condens. Matter* **25,** 252202 (2013).
36. Caillol, J., Levesque, D. & Weis, J. Theoretical calculation of ionic solution properties. *J. Chem. Phys.* **85,** 6645–6657 (1986).
37. Hlinka, J. *et al.* Coexistence of the phonon and relaxation soft modes in the terahertz dielectric response of tetragonal $BaTiO_3$. *Phys. Rev. Lett.* **101,** 167402 (2008).
38. Wang, D. *et al.* Fermi resonance involving nonlinear dynamical couplings in $Pb(Zr,Ti)O_3$ solid solutions. *Phys. Rev. Lett.* **107,** 175502 (2011).
39. Wang, D., Weerasinghe, J. & Bellaiche, L. Atomistic molecular dynamic simulations of multiferroics. *Phys. Rev. Lett.* **109,** 067203 (2012).

Acknowledgements

D.W. and L.B. acknowledge the support of the Air Force Office of Scientific Research under Grant FA9550-16-1-0065 and ONR Grant N00014-12-1-1034. A.A.B. and Z.G.Y. thank the ONR (Grant No. N00014-12-1-1045) and the NSERC (Grant No. 203773) for support. J.H. thanks the Czech Science Foundation (Project 15-04121S). D.W. also acknowledges the support from National Natural Science Foundation of China (Grant Nos. 51390472 and 11574246). Note that Z.G.Y.'s primary affiliation is Simon Fraser University.

Author contributions

D.W., A.A.B. and L.B. conceived this study with helpful input from J.H. and Z.-G.Y. D.W. performed molecular dynamics simulations. D.W. and A.A.B. analysed the dielectric responses. D.W., A.A.B. and L.B. wrote the first draft of the manuscript. All authors contributed extensively to the interpretation of the results and to the revision of numerous versions of the manuscript until its completion. D.W. and A.A.B. contributed equally to this work.

Additional information

Supplementary Information accompanies this paper at http://www.nature.com/naturecommunications

Competing financial interests: The authors declare no competing financial interests.

Reprints and permission information is available online at http://npg.nature.com/reprintsandpermissions/

How to cite this article: Wang, D. *et al.* Subterahertz dielectric relaxation in lead-free $Ba(Zr,Ti)O_3$ relaxor ferroelectrics. *Nat. Commun.* 7:11014 doi: 10.1038/ncomms11014 (2016).

This work is licensed under a Creative Commons Attribution 4.0 International License. The images or other third party material in this article are included in the article's Creative Commons license, unless indicated otherwise in the credit line; if the material is not included under the Creative Commons license, users will need to obtain permission from the license holder to reproduce the material. To view a copy of this license, visit http://creativecommons.org/licenses/by/4.0/